Image-Based Penetration Monitoring of CO_2 Laser Beam Welding

Characteristics of the weld pool and plasma plume as viewed through a dual-camera system indicate degrees of weld joint penetration

BY R. K. HOLBERT, R. W. RICHARDSON, D. F. FARSON AND C. E. ALBRIGHT

ABSTRACT. A dual-camera video system was developed to provide real-time information about the penetration modes of CO_2 laser beam welding for process quality monitoring and control. An experiment was designed to vary the penetration modes during welding by continuously changing the focal point position at different power levels and travel speeds. A study of the video images of the weld pool/keyhole region identified three types of weld pools: flat, depressed and keyhole. Images of the plasma plume revealed that a wispy, diverging fantail-shaped plume corresponded to the steady-state, flat and weakly depressed weld pools. As the power density and weld penetration depth increased, the diverging fantail plume changed to a concentrated columnar shape. A keyhole cavity was initiated when the diameter of the base of the columnar plume at the coupling spot (beam/material interaction site) and the calculated beam spot size were identical. Video images of the events during transition into and out of the keyhole mode from two vantage points were studied to identify features indicative of the presence of a keyhole. Keyhole welds were associated with a very intense columnar plume, elevated weld pool rim and several other visual cues. The unique perspective produced by the dual-camera video system could provide the basis for an in-process penetration control strategy and add to understanding of the physical processes that affect laser welding penetration mode and pool/plume dynamics during CO_2 laser welding.

R. K. HOLBERT is with Siemens Westinghouse Power Corp., Orlando, Fla. R. W. RICHARDSON, D. F. FARSON and C. E. ALBRIGHT are with The Ohio State University Department of Industrial, Welding and Systems Engineering, Columbus, Ohio.

Introduction

An important feature of continuous-wave, carbon dioxide (CO_2) laser welding is the ability to vary power density on the material surface over wide ranges by varying beam focus and power. Focusing the beam to a very small, high-power-density spot leads to the formation of a vapor cavity and a deep, narrow "keyhole-mode" weld. The high travel speeds and low thermal distortion associated with this welding mode give keyhole laser welding important advantages over other welding processes in certain applications. On the other hand, shallow conduction-mode laser welds generated at lower power densities are advantageous for surfacing applications where minimal penetration is usually desired.

The welding mode and the weld penetration depth in either mode are determined primarily by power density at the material surface, travel speed, base material properties and gas shielding. Since a number of these process inputs are susceptible to variation, process monitoring and feedback control to ensure proper welding penetration would be beneficial. In-process measurement of the laser welding mode (whether keyhole or conduction) and penetration depth is currently not possible, but it is vital for successful monitoring and control implementation. These measurements are difficult because of the small size of the laser weld, the harsh environment (smoke, spatter, high temperatures, etc.) and the practical need to make measurements from the topside of the work. Thus, developments in welding mode and penetration depth measurement are critical to the improvement and increased application of in-process laser weld monitoring and control capability. In this investigation, real-time images of the weld pool, keyhole and plume are analyzed to determine what weld mode and penetration information can be extracted from them.

KEY WORDS

Keyhole Mode
CO_2 Laser
Camera System
Monitoring
Conduction Mode
Weld Penetration

Laser Weld Penetration Monitoring

Techniques that provide direct in-process measurements of laser weld penetration (such as X-ray or ultrasonic sensing) have not been developed to the point that they are generically practical for industrial use. Thus, a popular approach (and the approach taken in this work) is to make measurements of other welding process information that is related to penetration and then infer the state of penetration from these measurements. Past work has been directed at analysis of

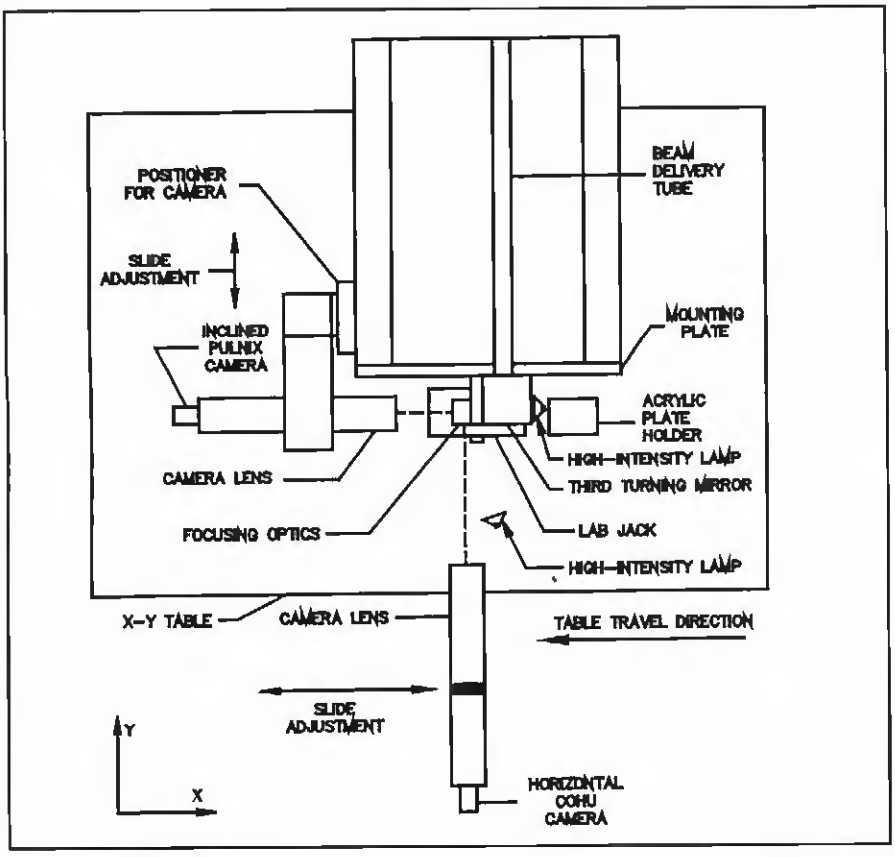

Fig. 1 — Top view of the video imaging equipment.

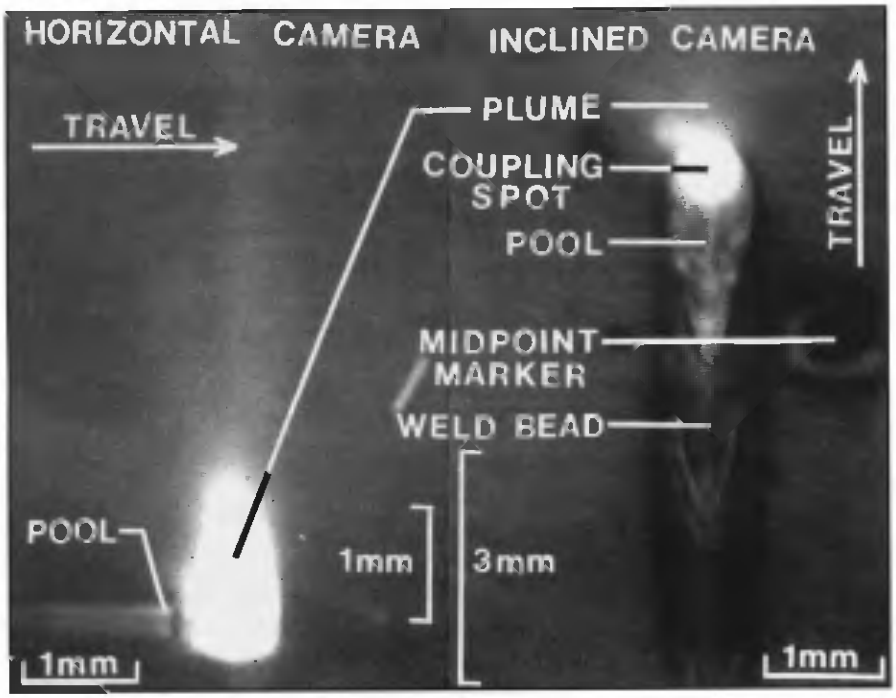

Fig. 2 — Split-screen video image of a 2-kW test weld (7.62 m/min) with the left image supplied by the horizontal camera and the right image supplied by the inclined camera.

acoustic and optical emissions (Refs 1–3), plasma charge emissions (Refs. 4, 5) and video images of the laser weld pool region. This short review concentrates on the latter since it is most relevant.

Denney and Metzbower (Ref. 6) describe a video system that visually monitors a CO_2 laser welding process. A pulsed, nitrogen laser was synchronized with a charged-coupled-device (CCD) camera to illuminate the weld area for the video images. A narrow-band line filter was used with the camera to allow only the nitrogen laser light (337 nm) to be received by the camera. Elimination of the effect of the plume intensity was not entirely achieved by nitrogen laser light, but the keyhole opening is clearly visible in the recorded images. Voelkel and Mazumder (Ref. 7) report a similar monitoring system that uses a continuous-wave argon laser (488 nm) for illumination. This system was used primarily for surface topography measurements, and the observations were made on shallow penetration laser welds.

Bagger, *et al.* (Ref. 8), describe a video system that was used to determine the penetration characteristics of the CO_2 laser welding of steel in a lap-joint configuration. The system had two CCD cameras providing images of the top and bottom of the weld. The images in their report are clear because an R66 filter (transmitting wavelengths above 660 nm) was used with the topside camera along with a high-intensity lamp for suppressing the intensity of the plume emissions. A green filter was used with the camera mounted backside. Schimon and Mazumder (Ref. 9) used a video system to monitor the interface width of laser lap welds in sheet metal. A CCD camera with external laser illumination was used to obtain measurements of weld bead top width. A number of welds were made over a matrix of power and travel speeds. An empirical relation was fit between the weld top widths and lap-joint interface widths, allowing on-line prediction of interface weld width.

Experimental Apparatus and Procedures

A video system previously developed at The Ohio State University (Ref. 10) was modified to a two-camera system design providing real-time images of the CO_2 laser pool and plasma plume. To investigate the capabilities of this two-camera video system, an experiment was designed to systematically analyze the phenomena occurring during penetration

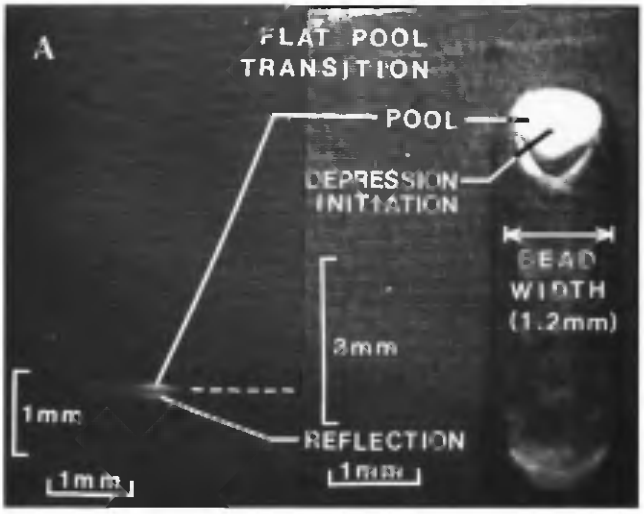

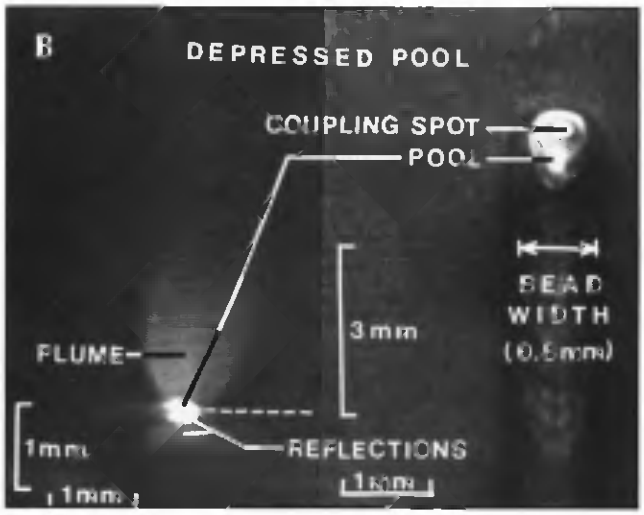

Fig. 3 — Transition from a flat weld pool to a depressed weld pool from a 1.5-kW test weld (2.03 m/min). A — Flat pool image; B — depressed pool image.

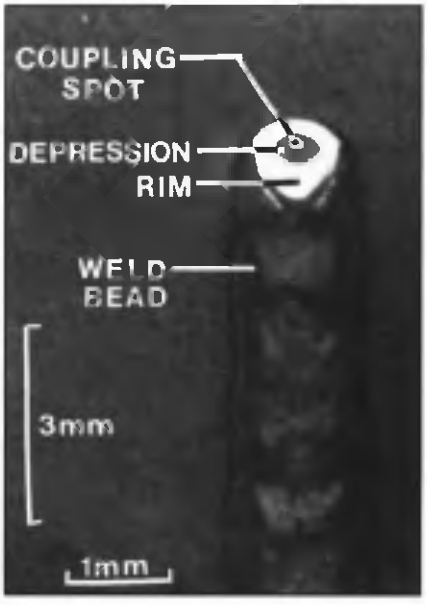

Fig. 4 — Inclined-camera image of a depressed pool from a 1.5-kW test weld (2.03 m/min) showing the coupling spot, the depression and the pool rim.

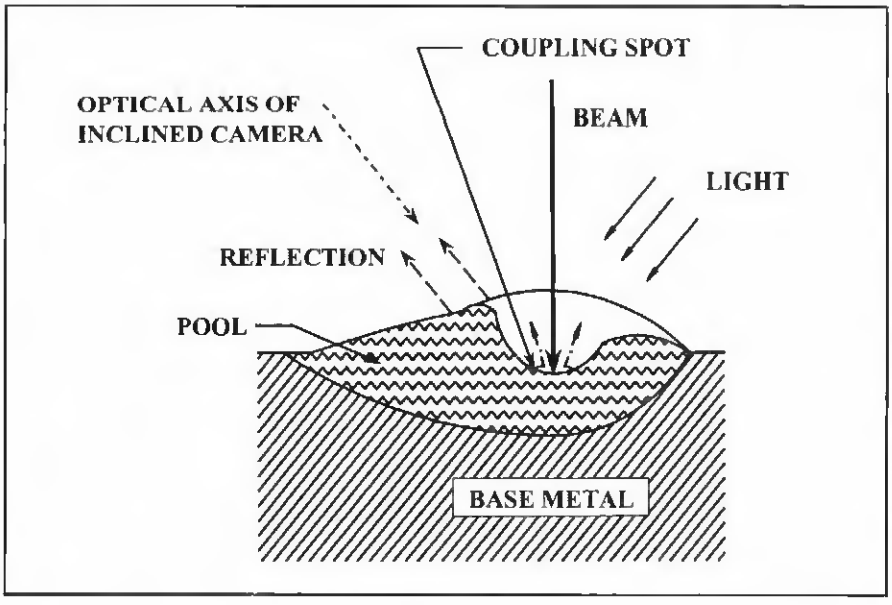

Fig. 5 — Depressed weld pool characteristics.

mode transitions from the video images. Recorded video images captured the dynamic behavior of the plasma and weld pool with power density change and resulting mode transition along the weld.

Video System

The video system recorded images from two camera systems (including CCD cameras, long-distance microscopic lenses and optical filters) and displayed them on a split monitor screen for simultaneous viewing of the weld process from two angles to facilitate analysis. Images from an inclined camera (mounted above and behind the weld at 45 deg to the beam axis in the direction of weld motion, as illustrated in Fig. 1) primarily provided information about pool characteristics, while images from a horizontal camera (mounted transverse to the direction of motion, as illustrated in Fig. 1) contained information about the plasma plume.

Both cameras used long-distance microscopic lenses with an approximate working distance of 305 mm. The camera/lens combination allowed a microscopic observation from a safe distance, protecting the camera and lens from smoke and spatter emitted by the weld. The shutter speed of the inclined camera was $\frac{1}{1000}$ s and that of the horizontal camera was $\frac{1}{2000}$ s. The video frame rate was fixed for both cameras at 30 interlaced frames/s. Quartz projector lamps of 300 W were used to overpower the plasma and thermal emissions so the weld pool could be observed clearly. One lamp was placed above the horizontal camera to illuminate the sample's surface, as shown

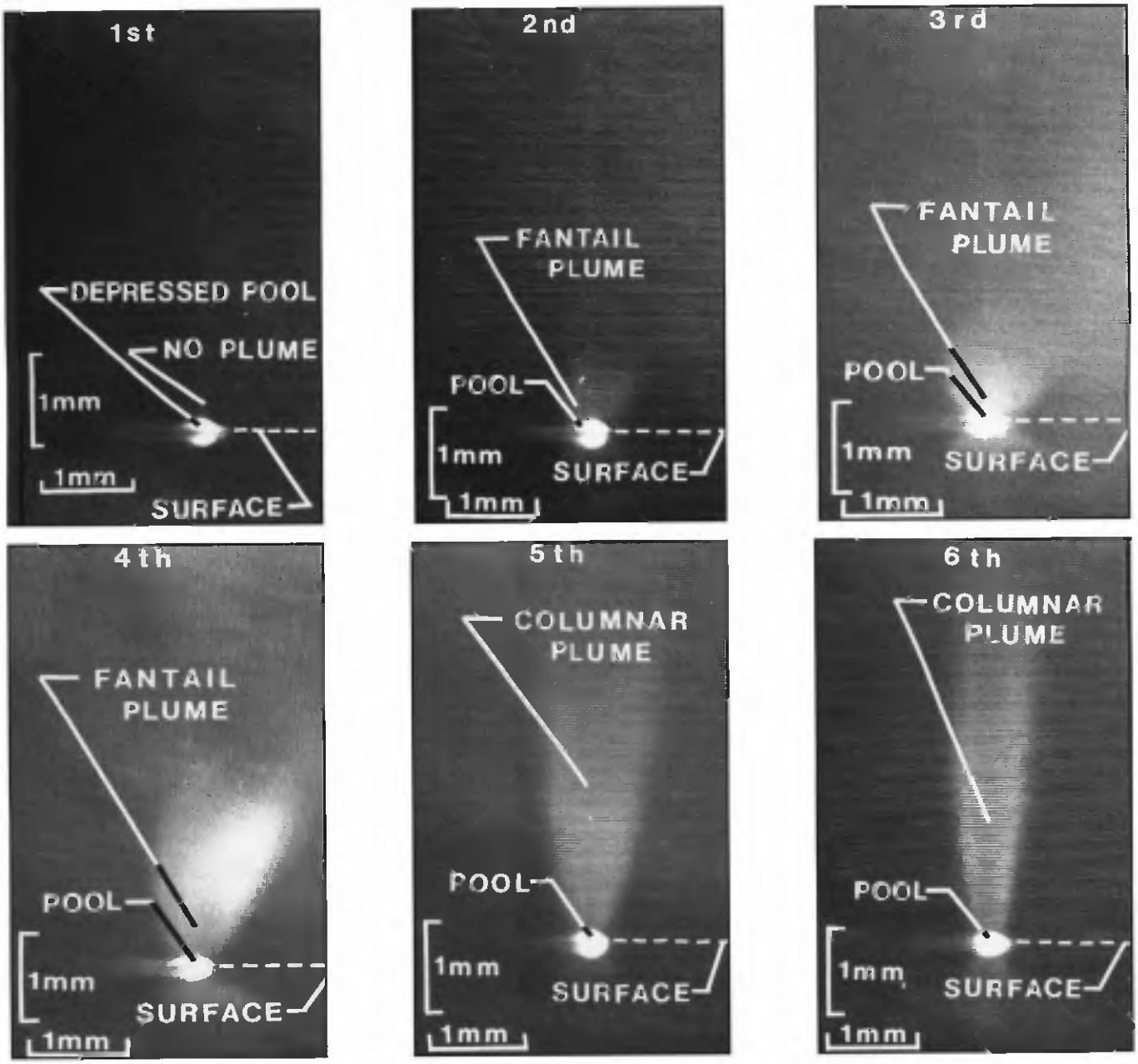

Fig. 6 — Horizontal camera images of plume pattern variations above the depressed pool of a 1.5-kW test weld (2.03 m/min) as the focal point moves closer to the surface.

in Fig. 1. The other lamp was mounted opposite to the inclined camera, also at a 45-deg angle in the weld-axis/beam-axis plane. This lamp provided oblique illumination of the weld area at the angle of maximum specular reflection from the sample surface to the inclined camera to brighten the background area around the intense glow of the plasma and molten metal. The horizontal lamp was less effective for illuminating the background because of its placement, but it did illuminate the weld pool during the tests. A 650-nm (±10 nm) narrow-band pass interference filter was used with the inclined camera. This filter passed the reflected, high-intensity light from the illuminator and blocked much of the keyhole plasma emission that consisted primarily of blue visible light (as determined by the unaided eye). Only a No. 2 neutral density filter was used with the horizontal camera to attenuate the plume light intensity.

The laser apparatus was a 3-kW, CO_2 laser with three programmable axes of motion. The laser equipment included a motorized Z axis that positioned a 150-mm reflective optic for beam focusing relative to the workpiece. Two other rectilinear axes provided part motion under the laser beam. The focal point position could be adjusted during the test weld, and reflective focusing optics minimized the fluctuation of the position caused by thermal distortion of the optic material. Helium shielding gas flowed across the entire top surface of the base material from a plenum incorporated into the weld fixture.

The beam power and travel speed were set prior to each test weld. Type 304 stainless steel sheet samples of thickness 1.5, 3.0 and 6.2 mm were used to obtain both partial and full penetration welds at different power levels. The focusing optics position was varied continuously during each test weld to change the power

density at the sample surface, producing transitions in weld penetration mode. Penetration mode transitions were from shallow, conduction-mode penetration at the weld start to keyhole-mode penetration in the middle, reverting back to conduction-mode near the end of weld. The standoff change magnitude was selected to produce a keyhole weld over roughly one third of the total weld length.

The experimental design was a three-by-five test matrix (three power levels at five travel speeds for each sample thickness), which provided the high and low extremes with some midpoint parameters in the practical envelope of operation, as presented in Table 1. To eliminate any systematic bias in the statistical design of the experiment, test welds were conducted in random order. Each test involved a continuous change of laser beam focus position from above (+) to below (–) the sample's surface. Samples of different thickness were not randomized in the experimental sequence since the change from one thickness to another required a significant amount of setup time.

Focal point position relative to the material surface was measured before each test weld using an acrylic plate beam imprint as described by Arata (Ref. 11).

Results and Discussion

A unique characteristic of the dual-camera video system was its ability to provide observations of the weld pool and plume from two vantage points at approximately the same time. Recorded images capture the changes in the plume and pool during the penetration mode transitions. Figure 2 shows a typical split-screen display of the two-camera image of a laser weld in the keyhole penetration mode.

The left image in Fig. 2 is from the horizontal camera that provided observations of the weld pool and plume transverse to the weld axis. From this viewpoint, the leading edge of the pool in the horizontal-camera image is to the right. The dominant feature in a typical horizontal-camera image is the laser plume, but the molten pool can also be seen protruding above the sample's surface (to the left of the plume). Magnification of these features in the horizontal-camera image was approximately 31:1 of the actual proportions (scale bars are shown to allow estimation of the magnification as-published). The transitions of the plume during the tests are distinct in the horizontal-camera, image but detailed study of the time variation of the plume was precluded by the slowness of the frame rate (30 Hz) relative to plume variation frequencies (which are known to range up to about 15 kHz). The camera used in this investigation "averaged out" the high-frequency plume variations.

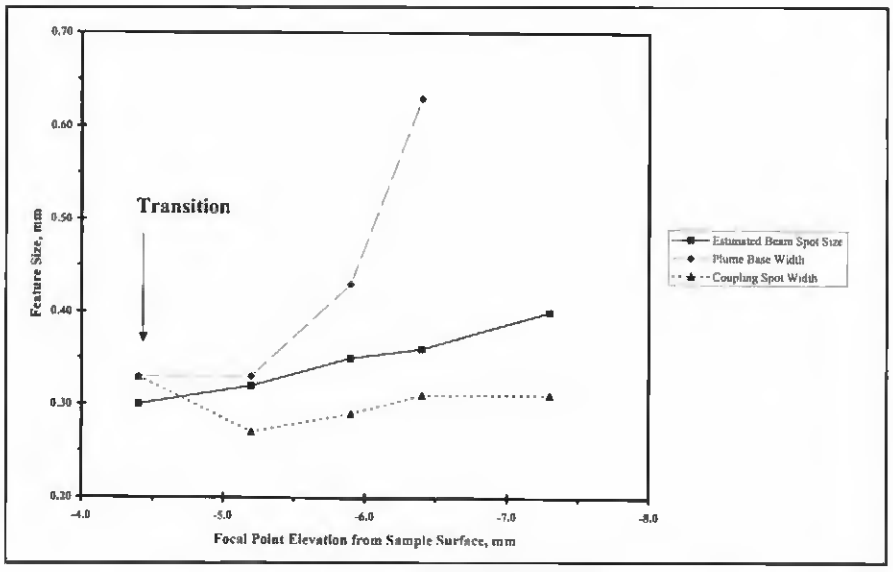

Fig. 7 — Change in the plume base and coupling spot dimensions with increasing beam spot size for a 1.5-kW test weld (2.03 m/min), showing a transition to keyhole mode when the three are roughly equal.

The right image of the video output in Fig. 2 is from the inclined camera with the optical axis at a 45-deg angle from vertical and to the rear of the weld. This camera provides observations of the top of the pool, and the plume is also visible due to the angle of the optical axis. The leading edge of the pool and the direction of travel is toward the top of the inclined-camera image. Some foreshortening of the vertical dimensions of the image results from the angle of inclination; the corrected vertical magnification of the features in the inclined image was approximately 21:1 of the actual dimensions. The magnification of horizontal features in the image was 32:1 of the actual size. A feature that will be termed the "coupling spot" is also labeled in this camera view. In this article, the term coupling spot is used to refer to the highly luminous area where the beam is absorbed by the molten material and its vapor. In keyhole welding mode (which is studied in more detail later), it corresponds to the cavity opening. The coupling spot and the beam spot (intersection of the focused beam and the surface of the workpiece) are also related but are not necessarily identical. Since the plume originates from the coupling spot, the width of the base of the plume and the diameter of the coupling spot should be comparable in the two images. The diameter of the plume base along the X axis in the horizontal-camera image in Fig. 2 is 0.9 mm, which correlates closely with the width of the coupling spot in the inclined-camera image (0.9 mm).

Table 1 — Summary of the Test Parameters Used for the Experimental Welds

Sample Thickness, mm	Beam Power W	Travel Speed m/min	Focal Point Position Relative to the Surface of the Sample
1.5	700	0.25	From
	1100	1.02	+7.6 (above)
	1500	2.03	
		3.81	To
		7.62	–7.6 (below)
3.0	1100	0.25	From
	1500	1.02	+10.2 (above)
	2000	2.03	
		3.81	To
		7.62	–10.2 (below)
6.2	1500	0.25	From
	2000	1.02	+12.7 (above)
	2500	2.03	
		3.81	To
		7,62	–12.7 (below)

Analysis of Conduction-Mode Weld Pool Images

Three distinct weld pool types were identified from the video observations: flat, depressed and keyhole. The first two both fall under the heading of conduction mode welds. These were generated by changes in power density due to the variation of the focal point position during the tests. The smooth, flat pool occurred when the focal point position was

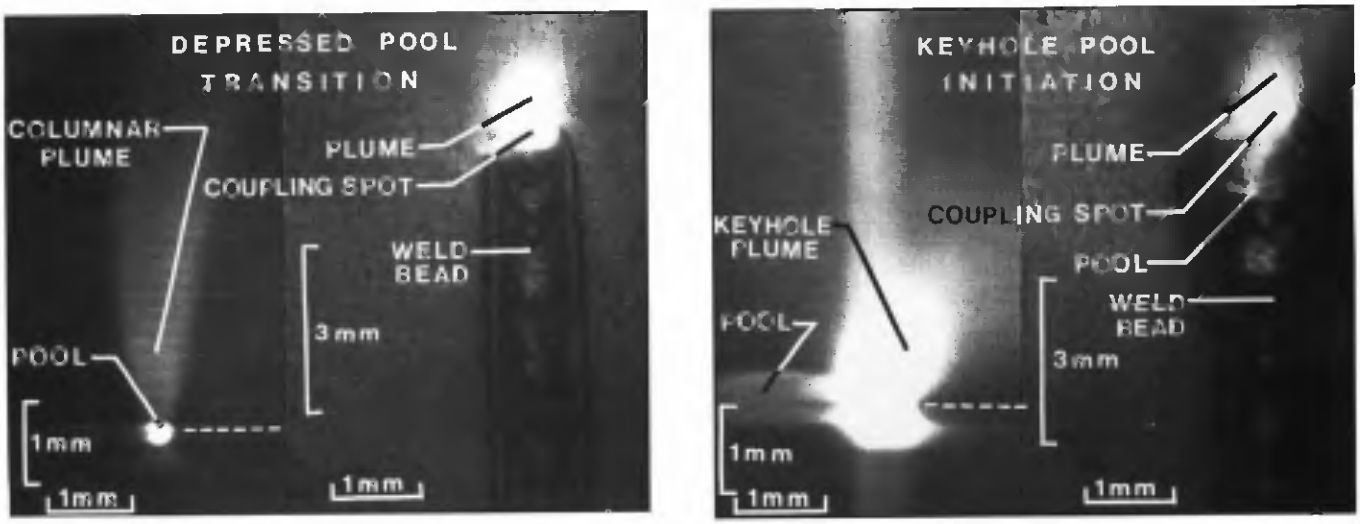

Fig. 8 — The transition from a depressed pool to a keyhole pool for a 1.5-kW test weld (2.03 m/min). A — Depressed pool image; B — keyhole pool image.

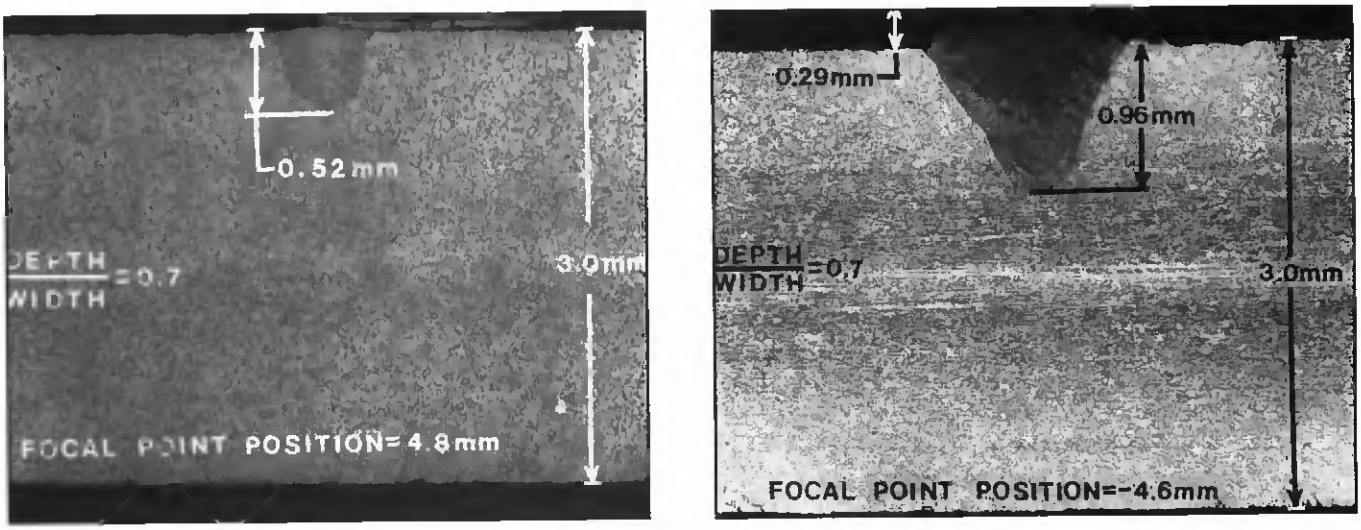

Fig. 9 — Weld cross sections corresponding to plume images shown in Fig. 8. A — Depressed weld; 8 — keyhole weld.

far from the sample's surface, resulting in a low-beam power density. As the focal point approached the sample surface, beam power density increased, creating a gradually deepening depression in the molten pool, which was visible in both camera views. In cases where maximum power density was sufficiently high, an abrupt transition to a keyhole weld with a large, turbulent pool was observed.

Video recordings showed a depressed pool occurred in all of the test welds. Figure 3 shows the transition from a flat pool to a depressed pool in a 1.5-kW test weld. The pool in the top horizontal-camera image of Fig. 3 is flat with an insignificant pool height. A small depression just forming in the molten pool is seen as a faint, dark semicircle in the pool (barely visible in the inclined-camera image of the top photograph). The dark area denotes an inclined surface that reflects light away from the inclined camera. A uniform, specular reflection is characteristic of the remainder of the pool, which is interpreted as a smooth surface. No plume was visible over the flat pools, but as power density increased and the pool surface became depressed, a faint plume appeared and gradually increased in brightness. In most cases, propagation of the columnar plume was not exactly along the beam axis but slightly tilted away from the axis. The weld pool in the bottom horizontal-camera image (after the flat-to-depressed transition) is an elliptical glow 0.2 mm above the sample surface with its reflection below the surface. In the bottom inclined-camera image of Fig. 3, the leading portion of the slender teardrop-shaped depressed pool contains the coupling spot and the depression with a uniformly smooth surface in the aft section of the pool. The bottom horizontal-camera image in Fig. 3 shows a wispy fantail-shaped plume

The transition to a depressed pool was somewhat erratic. The depression in the pool generally formed, disappeared and reformed a number of times before achieving a stable depressed-pool state. A decrease of the weld bead width (from 1.2 to 0.8 mm) occurred with the transition from a flat pool to a depressed pool. Initially, the weakly depressed-pool plume had a fantail shape, which evolved into a columnar shape as the power density increased. Stabilization of the depressed pool generally occurred

when the plume was visibly present.

In the depressed-pool images from both cameras, the features of primary interest are the plume, pool and coupling spot. Observations of the plume could be made from the horizontal and inclined images. The pool was also identifiable in both camera images, but the coupling spot was visible only in the inclined-camera images. The depressed pool appeared to be concave at the CO_2 laser beam/material interaction location. This observation agrees with the conclusions of Voelkel and Mazumder (Ref. 7) based on their video images of conduction-mode welds. Three regions of the depressed pool were identified in the inclined-camera images: the rim, the depression and the coupling spot. Figure 4 shows the coupling spot in the upper portion of the depressed pool surrounded by a dark band and then a very bright outer ring (teardrop shaped) in the inclined-camera image of a 1.5-kW test weld. The bright outer ring is interpreted to be the flat, tranquil upper rim of the pool, projecting above the sample's surface. Where the inclination angle of the depression walls is unfavorable for light reflection into the camera, a dark band can be seen in the pool. A bright nucleus is evident at the center of this dark depression. This bright spot is identified as the coupling spot and is accentuated in the darkness of the depression in the inclined-camera images.

Based on video images of depressed pools, the illustration in Fig. 5 depicts the depressed pool relative to the laser beam, the high-intensity lighting and the optical axis of the inclined camera. The outer portion of the molten pool forms a rim around the shallow depression, which is in the interior of the pool located near the leading edge. Since the coupling spot is at the center of the depression, the depression and coupling spot are apparently centered on the beam axis. This observation agrees with the findings of Voelkel and Mazumder (Ref. 7). Illumination of the rim is by the auxiliary lighting opposite the inclined camera. This light is specularly reflected toward the inclined camera, but the walls of the depression are not at the appropriate angle for reflection. Thus, the depression appears dark in the images with the bright coupling spot in the center. Figure 5 shows the highest location on the rim is on either side of the depression where the Y-Z plane passes through the beam axis. The center of the coupling spot and the lowest point in the depression occur at the intersection of the beam axis and this Y-Z plane. It appears that this location on the rim is composed of the displaced molten metal from the depression in the pool.

Figure 6 shows six successive (but noncontiguous) horizontal-camera images of the plume transformation over the depressed pool for a 1.5-kW test weld with a travel speed of 2.03 m/min. During the time spanned by the six images, the focal point position approached the surface from an elevation of +10 mm (above the surface) in the first image to +4 mm in the last image. There was no plume present in the first image when the pool initially changed from the flat pool to a depressed pool. A slightly crowned appearance of the pool is the only indication the pool was not completely flat.

The focal point position was closer to the surface in the second image, and the increased power density resulted in the formation of a weak, wispy, fantail-shaped plume over the depressed pool. In the third and fourth images, the fantail plume developed into a more distinct vapor cloud and began to increase in height as the spot size became continuously smaller. Finally, the fantail plume concentrated into a columnar shape, as seen in the fifth image. The sixth image shows the weld just before initiation of the keyhole cavity, when the beam waist was 4.0 mm above the material surface. The columnar plume was more slender and slightly taller than in the previous images. No significant change was observed in the diameter of the coupling spot throughout the sequence, even though the beam spot size and the width of the plume base decreased.

During the image sequence shown in Fig. 6, cross section measurements (repeated for two welds with the same parameters) revealed the weld pool penetration increased from 0.38 mm to 0.52 mm. Thus, the plume shape (divergence angle) and height are both observables that could correlate to power density and weld depth in conduction-mode welds. Additional tests are required to quantify the relationship and determine the accuracy of penetration estimates obtained from plume-shape measurements.

Comparing the sizes of the various features in the conduction-mode weld images, a relationship that consistently predicted the transition to or from keyhole-mode welding was noted. Figure 7 summarizes this result. The figure plots the dimensions of three features measured in a sequence of images taken as a weld transitioned from keyhole to depressed mode when the focal position moved from –4.4 to –7.3. Prior to the welding mode transition, the coupling spot diameter, estimated beam spot diameter and plume base diameter were all approximately equal. This relationship is potentially useful in determining when a weld is about to switch in or out of keyhole mode.

Comparison of Keyhole- and Conduction-Mode Weld Images

Image observables that are potentially useful for detecting keyhole weld formation were determined by studying pictures taken just before and after the transition to and from keyhole welding. Figure 8 shows one video image taken just at the instant of the depressed-to-keyhole transition and another a few video frames later. Figure 9 shows weld cross photographs corresponding to the plume images in Fig. 8. A columnar plume is evident in the horizontal-camera image and is representative of the depressed pool prior to the keyhole cavity formation. However, an intense glow denotes a keyhole plume was beginning to develop in the inclined-camera image. The weld cross section in Fig. 9A shows a very deeply depressed conduction mode weld pool. Images at the bottom of Fig. 8 show the keyhole pool and plume as they were beginning to stabilize. An extremely bright, dynamic keyhole-pool plume (in the horizontal-camera image) signified the formation of the keyhole cavity. Also, the pool height increased significantly during the stabilization of the keyhole cavity, appearing as a "rooster-tail" wake behind the coupling spot. This wake is presumably formed by displacement of the molten material from the keyhole cavity. It also causes turbulence in the molten pool resulting in the "ruffled" appearance. The bottom inclined-camera image in Fig. 8 shows that the pool widened dramatically and the pool shape changed from a small teardrop of the depressed pool to a large, uneven elongated ellipse of the keyhole pool. Keyhole initiation also resulted in the increase of the coupling spot dimensions. The corresponding keyhole-mode weld cross section in Fig. 9B confirms the dramatic increases in weld width and depth that were associated with the onset of keyholing.

In summary, both the plume shape and intensity, as well as the measured weld pool height, were clear indications of whether or not the weld was in keyhole mode. Pool width and surface appearance also appeared to be potentially useful for this purpose.

Conclusions

The investigations using the video system and weld images led to the conclusions below.

1) The dual-camera video system developed during this investigation successfully produced simultaneous, high-resolution images from two vantage points. The cameras and optics were located at a sufficient distance from the heat and debris caused by laser material processing that they could be the basis of a practical penetration control system. Other restrictions, such as access to the weld location, might also have to also be accomodated during practical implementation of such a system for a specific application.

2) As observed in the horizontal-camera images, decreasing focus spot size generated a fantail-to-columnar plume shape transition. Just before keyhole initiation, the columnar plume was much more intense and distinct than the original fantail plume of a weakly depressed pool.

3) A potentially useful correlation was noted between nonkeyhole weld pool penetration and the divergence, height and intensity of the plume

4) Dimensions of selected depressed-pool image features were found to be related to the formation and termination of the keyhole cavity. The width of the columnar plume base, coupling spot width and estimated beam spot size, were approximately equal immediately before and just after transition to and from keyhole welding mode.

5) Keyhole welds were differentiated from flat or depressed pools in the images by much brighter plumes with larger variations in size and shape and much larger pool heights as measured in the horizontal view.

Acknowledgments

We express our gratitude to Edison Welding Institute, especially Karl Graff and Dave Edmonds, for allowing us to use their laser system and equipment to conduct this research. We appreciate the contributions of Bob Rivett, John Lippold, Gene White, Jim Hurley, Scot Leonard, Larry Stahr, Tim Freck, Ed Robitz and Dan Gibson on the experimental procedure. The advice of David Whitehouse and Stan Ream concerning the measurements of beam quality are valued.

References

1. Farson, D., Ali A., and Sang, Y. 1998. Relationship of optical and acoustic emissions to laser weld penetration. *Welding Journal* 77(4): 142-s to 148-s.

2. Farson, D., Sang, Y., Ali, A. 1997. Relationship between air-born acoustic and optical emissions during laser welding. *Journal of Laser Applications* 9(2): 87–94.

3. Farson, D., Hillsley, K., Sames, J., Young, R. 1996. Frequency-time characteristics of air borne signals from laser welds. *Journal of Laser Applications* 8(1): 33–42.

4. Farson, D., Ali, A., Li, X. C. 1999. Laser weld penetration monitoring with multiple emission signal measurements. *Journal of Laser Applications*, (in press, to appear in April).

5. Li., L., Brookfield, D. J., Steen, W. M. 1996. Plasma charge sensor for in-process, noncontact monitoring of the laser welding process. *Measurement Science and Technology*, no. 7, pp. 615–626.

6. Denney, P. E., and Metzbower, E. A. 1991. Synchronized laser-video system study of high-power laser material interactions, ICALEO '91 Vol. 74 — Laser Material Processing, *Proceedings of the Tenth International Congress on Application of Lasers and Electro-Optics*, eds. E. A. Metzbower, E. Beyer and A. Matsunawa, pp. 84–93. Laser Institute of America, Toledo, Ohio.

7. Voelkel, D. D., and Mazumder, J. 1991. Visualization and dimensional measurement of the laser weld pool. ICALEO '90 — Laser Materials Processing, *Proceedings of the Ninth International Congress on Applications of Lasers and Electro-Optics*, eds. S. L. Ream, F. Dausinger and T. Fujioka, pp. 423–429. New York, N.Y., IFS Publications.

8. Bagger, C., Miyamoto, I., Olsen, F., and Maruo, H. 1991. On-line control of the carbon dioxide laser welding process. *DVS, 135 (Strahltechnik)*, pp. 1–6.

9. Schimon, R. W., Mazumder, J. 1993. Monitoring of interface width during laser lap welding through visualization. ICALEO '93 — Laser Material Processing, *Proceedings of the 12th International Congress on Application of Lasers and Electro-Optics*, pp. 382–392. Laser Institute of America, Toledo, Ohio.

10. Holbert, R., and Richardson, R. 1990. A vision-based sensor for laser welding. Presented at the Seventy-First Annual American Welding Society Convention in Anaheim, Calif., April 25, 1990.

11. Arata, Y. 1986. Evaluation of beam charateristics by the AB test method. *Plasma, Electron, and Laser Beam Technology*, ed. Y. Arata, pp. 177–193. ASM International, Materials Park, Ohio.

Call for Papers

The ASTM Committee on Reactive and Refractory Metals and Alloys invites papers for its International Symposium on Zirconium in the Nuclear Industry to be held June 10–14, 2001, in Annecy, France. The symposium provides a forum to exchange information on the fabrication, testing, development and characterization of zirconium-based materials in the nuclear industry.

Topics for papers might include, but are not limited to, the following: basic metallurgy, processing and fabrication, alloy development, mechanical behavior, primary failure mechanisms, degradation mechanisms of failed fuel, corrosion and hydriding, in-reactor performance, irradiation effects, high-temperature and transient phenomena and long-term storage.

Send a 250–300 word abstract and title of the paper, along with an ASTM paper submittal form, by May 15, 2000, to Dorothy A Fitzpatrick, Symposia Operations, ASTM, 100 Barr Harbor Dr., P.O. Box C700, W. Conshohocken, PA 19428-2959; tel. (610) 832-9677. Submittal forms are available from Fitzpatrick. Do not send abstracts by fax or e-mail.

Notification of paper acceptance will be by Sept. 15. Additional information is available from Committee Chairman Gerry Moan: tel. (905) 823-9060, ext. 3232; moang@aecl.ca.